Multimodal analysis for the stability of vortices with axial flow

Gennaro Coppola[1], Fortunato de Rosa[2], Luigi de Luca[2]
[1]*DETEC, Università di Napoli "Federico II", Italy*
E-mail: gcoppola@unina.it,

[2]*DIAS, Università di Napoli "Federico II", Italy*
E-mail: deluca@unina.it

Keywords: trailing vortices, hydrodynamic stability, non-normality.

SUMMARY. The problem of transient behavior of perturbations in the linear stability analysis of vortex columns with axial flow is considered. We use the Batchelor vortex as the base flow and the analysis is carried out by focusing on a region of the parameters space in which both weak viscous exponential instabilities and transient growths of perturbations are present. The competition between the two linear effects is analyzed in a certain range of axial and azimuthal wavenumbers. The numerical discretization has been performed by employing an accurate Chebyshev collocation spectral method. The computations of the growth function evolution and of the optimal perturbations have been conducted by implementing two different strategies, the matrix exponentiation and the direct-adjoint techniques, and a comparison in terms of computational cost and accuracy is presented. Furthermore, some aspects of the competition between viscous instabilities and transient effects, in a swirl numbers range in which are both present, are discussed.

1 INTRODUCTION

The stability of high Reynolds number swirling flows is a topic of major interest in hydrodynamic stability theory, applications ranging from aircraft trailing wakes to vortex breakdown in fully developed turbulence. Among the various available vortex solutions, the Batchelor (or q) vortex has been widely used as theoretical model, mainly for vortex wakes. The Batchelor solution is constituted by a gaussian azimuthal velocity profile in the presence of axial flow and is governed by a single parameter q measuring the swirl strength.

The modal instability of the Batchelor vortex has been investigated by several researchers over the past decades, for both inviscid [5, 6, 7, 8] and viscous flows [9, 10, 11]. The analysis has been carried out mainly by using numerical methods and the existence of two classes of exponential instabilities has been recognized. The first class is a family of strong inviscid instabilities affecting negative azimuthal wavenumbers and moderately low values of the swirl parameter ($q \leq 2.31$). Still at high Reynolds numbers, these instabilities are quickly damped for $q \geq 1.5$, while persist for lower values of the swirl parameters also for moderate Reynolds numbers. The second class is constituted by weak viscous modes which are present for all values of the swirl parameter at sufficiently high (but still finite) Reynolds numbers.

In addition to these families, recent investigations by Heaton and Heaton and Peake [3, 4] have shown the occurrence of transient growth of perturbations directly linked to an algebraic instability arisen as an effect of the inviscid continuous spectrum. These last studies extend the previous investigations on transient growth in isolated columnar vortices without axial flow performed by Antkowiak and Brancher [1] and by Pradeep and Hussain [2].

Despite the great attention devoted to the Batchelor model and the amount of theoretical and numerical results, the complete understanding of the breakdown process for vortices with axial flow

appears still far from being achieved. Since the Batchelor model is affected at sufficiently high values of the Reynolds number by strong exponential instabilities for moderately low values of the swirl parameter, the breakdown phenomenon needs an explanation particularly in this region of parameters. On the other hand, the flow is affected by both weak viscous instabilities and by transient growths, accordingly the mechanism of breakdown should emerge from the competition between these two effects. Incidentally, note that these values of parameters are the same occurring also for wake aircraft vortices, one of the principal applications of the Batchelor model.

Previous studies by Heaton and Peake [3] and Heaton [4] have performed a quite complete analysis of transient effects at all moderately high to infinite values of the swirling parameter, but only for moderate Reynolds numbers. The present paper attempts to clarify some aspects of the competition between viscous instabilities and transient effects by focusing on a lower range of the swirl parameter, where the exponential instability are present, and moderately higher Reynolds numbers.

2 GOVERNING EQUATIONS AND PARAMETERS

We work in cylindrical polar coordinates (r, θ, z) with corresponding unit vectors in the coordinate directions $(\mathbf{e}_r, \mathbf{e}_\theta, \mathbf{e}_z)$. Total velocity components and pressure are u_r, u_θ, u_z and p^* and the decomposition between base flow and perturbations takes the form:

$$(u_r, u_\theta, u_z, p^*) = (U, V, W, P) + (u, v, w, p)$$

where velocity and pressure perturbations are denoted by u, v, w and p. Fourier decomposition in azimuthal and axial directions leads to the position:

$$(u, v, w, p) = (\mathrm{i}\tilde{u}, \tilde{v}, \tilde{w}, \tilde{p})(r, t)e^{\mathrm{i}(kz+n\theta)}$$

where $k \in \mathbb{R}$ and $n \in \mathbb{Z}$ are respectively the axial and azimuthal wavenumbers. Following [11], we scale lengths on the vortex core radius and velocities on centreline axial velocity. With these positions, the Batchelor vortex base flow is:

$$U = 0 \qquad V(r) = \frac{q}{r}\left(1 - e^{r^2}\right) \qquad W(r) = e^{-r^2}$$

and the nondimensional complex disturbance equations, arising from linearized Navier-Stokes and continuity equations are:

$$0 = \mathcal{D}^*\tilde{u} + \frac{n\tilde{v}}{r} + k\tilde{w} \tag{1}$$

$$\mathrm{i}\frac{\partial\tilde{u}}{\partial t} = \Sigma\tilde{u} + 2\Omega\tilde{v} - \mathcal{D}\tilde{p} + \frac{\mathrm{i}}{Re}\left[\left(\nabla^2_{n,k} - \frac{1}{r^2}\right)\tilde{u} - \frac{2n}{r}\tilde{v}\right] \tag{2}$$

$$\mathrm{i}\frac{\partial\tilde{v}}{\partial t}\tilde{v} = \Xi\tilde{u} + \Sigma\tilde{v} + \frac{n\tilde{p}}{r} + \frac{\mathrm{i}}{Re}\left[\left(\nabla^2_{n,k} - \frac{1}{r^2}\right)\tilde{v} - \frac{2n}{r}\tilde{u}\right] \tag{3}$$

$$\mathrm{i}\frac{\partial\tilde{w}}{\partial t}\tilde{w} = W'\tilde{u} + \Sigma\tilde{w} + k\tilde{p} + \frac{\mathrm{i}}{Re}\nabla^2_{n,k}\tilde{w}. \tag{4}$$

In these equations $\mathcal{D}$ stands for derivative with respect to r, $\mathcal{D}^*$ is the polar derivative $\mathcal{D}^* = \mathcal{D} + 1/r$, $\nabla^2_{n,k}$ is the laplacian in cylindrical coordinates acting on a normal mode:

$$\nabla^2_{n,k} = \frac{1}{r}\frac{\mathrm{d}}{\mathrm{d}r}\left(r\frac{\mathrm{d}}{\mathrm{d}r}\right) - \frac{n}{r^2} - k^2$$

and prime denotes differentiation with respect to r for base flow. We set also the following positions:

$$\Sigma = nV/r + kW \qquad \Omega = V/r \qquad \Xi = \mathcal{D}^* V.$$

In order to perform classical modal analysis, the position is made, $\tilde{a}(r,t) = \bar{a}(r)e^{-\mathrm{i}\omega t}$, where a is any flow variable. The system (1-4) furnishes the eigenvalue problem usually employed for modal analysis by simply substituting partial derivative with respect to t with $-\mathrm{i}\omega$.

In the next sections we will need to compare our results with some published literature and to this end occasionally we will refer to the equivalent nondimensional variables (starred in the following) obtained by scaling velocity on the vortex swirl and defining the Reynolds number on the mean flow circulation at infinity (cfr. for example [3]). The conversions between the two scalings are the following:

$$V^*_{\text{ref}} = qV_{\text{ref}}, \qquad t^*_{\text{ref}} = qt_{\text{ref}}, \qquad Re^* = 2\pi qRe.$$

Boundary conditions are that perturbations decay to zero as $r \to \infty$ and that at the axis of the vortex (cfr. Ash & Khorrami [14] and Pradeep & Hussain [2]) it holds:

$$\begin{aligned}
&\tilde{u}, \tilde{v}, \mathcal{D}\tilde{w} = 0, \tilde{p} \text{ finite} \quad \text{for} \quad n = 0 \\
&\mathcal{D}\tilde{u}, \tilde{u} + n\tilde{v}, \tilde{w}, \tilde{p} = 0 \quad \text{for} \quad |n| = 1 \\
&\tilde{u}, \tilde{v}, \tilde{w}, \tilde{p} = 0, \quad \text{for} \quad |n| > 1.
\end{aligned}$$

In order to define the energy of the perturbation and the growth function $G(t)$, we need a definition for the scalar product, which we choose to be the standard inner product:

$$< f, g >= \int_0^\infty f^* g r \, dr. \tag{5}$$

The energy of a disturbance is hence defined by $E(t) = 1/2\|(\bar{u}, \bar{v}, \bar{w})\| = 1/2 < (\bar{u}, \bar{v}, \bar{w}), (\bar{u}, \bar{v}, \bar{w}) >$ and the growth function is defined at each time as the maximum energy amplification over all the initial conditions of unit norm.

3 NUMERICAL TREATMENT AND VALIDATION

3.1 *Numerical treatment*

The system of equations (1-4) and the corresponding eigenvalue problem for modal analysis, has been discretized by a Chebyshev pseudospectral code written in MATLAB programming language. The semi-infinite domain is mapped to the interval $[-1, 1]$ via the general transformation:

$$r = C\frac{1+x}{1-x^\beta}$$

which reduces to the mapping function employed in [3] for $\beta = 1$. In most cases by setting $C = \beta = 1$ the desired accuracy could be achieved; occasionally we took advantage of the additional parameters C and β in order to obtain more accurate results. We make use of the DMSUITE package by Weideman & Reddy [16] in order to obtain the discretized differential operators. Boundary conditions are enforced by replacing rows.

The system of equations has been discretized in various forms in order to obtain eigenvalues ω for various parameters values. Apart from the form (1-4), involving the four variables $\tilde{u}, \tilde{v}, \tilde{w}, \tilde{p}$, other versions of the model have been discretized, which involve the state variables $(\tilde{u}, \tilde{v}, \tilde{w})$ and $(\tilde{u}, \tilde{v})$ and three or two equations respectively. These versions are obtained by eliminating $\tilde{p}$ and

$\tilde{w}, \tilde{p}$ respectively and are reported in various papers (cfr. [3, 2, 11]). We found that, by accurately programming the higher order operators, the best results in term of spectral accuracy and computational time are achieved by the two-equations version of the model; in what follows all the computed results related to eigenfunctions have been obtained with this model and by suitably adjusting the parameters C and β in the mapping function.

The spectral discretization of the spatial operators in eq. (1-4) has been employed also for the implementation of the techniques for the computation of transient growth. We implemented both the "direct-adjoint" technique and the "matrix exponentiation" technique. For what it concerns the direct-adjoint technique, we followed, *mutatis mutandis*, the procedure outlined in [3]. We employed the two equations model for the state vector (u, v) and its corresponding adjoint equations system, obtained by considering the scalar product (5). For time integration we employed a first order implicit Euler time discretization and typically $N = 100 \div 150$ spatial discretization points. Further details on this technique and on the relevant associated definitions are not reported here, the reader being referred to [2] and [3].

Matrix exponentiation technique has been adapted from Schmid & Henningson textbook [15]. We found that the most reliable model from a computational point of view is the one constituted by the four equations (1-4), without any substitution. The reason for this seems to lie in the fact that in order to obtain converged transient growth functions and optimal perturbations, a great number of "non-converged" eigenvalues (whose number and location in the complex plane is strongly dependent on the number of collocation points) needs to be included. In fact, although counter-intuitive, these 'spurious' modes, lying usually on a double zip-fastener branch near the upper margin of the stable half complex plane and with associated eigenfunctions having a mesh-dependent sawtooth aspect, are globally representative of some physical effect since, when combined in superposition, they give a converged result. These modes are increasingly far from being resolved as the order of the differential operators grows. These modes are poorly resolved also in the discretization of the basic form (1-4) but, surprisingly enough, when included in the optimization procedure they lead to converged growth functions. It is certainly a very interesting phenomenon, which don't seems fully understood, that the convergence of the individual modes is a different matter to the convergence of superpositions of modes but, on the other side, a similar behavior has been encountered in different contexts and some further comments on this topic can be found in the recent paper by Heaton *et al.* [12]. Despite these difficulties, by accurately checking the results obtained with the alternative "direct-adjoint" technique, we were able to extract maximum growth factors for Reynolds numbers up to 10^5.

3.2 VALIDATION

The spectral code has been validated by recalculating all the existing data in the published literature on both Batchelor and Lamb-Oseen vortex models. The agreement between our results and published data is generally excellent. Complex mapping functions have been employed in cases in which difficulties are encountered for real mappings and also in these cases we were able to reproduce accurately all the published results.

We calculated also transient growth of perturbations for selected parameters values for the case of the Batchelor vortex. The validation of our codes has been made by re-calculating transient growth results contained in [13] for the Hagen-Poiseuille base flow and in [3] and [4] for the Batchelor vortex. The results are quite good for the direct-adjoint technique at moderate Reynolds numbers, although the requirement of higher accuracy in long time integrations and ill conditioning of the spectral discretization of the evolution operators renders this technique quite cumbersome. In Fig. 1

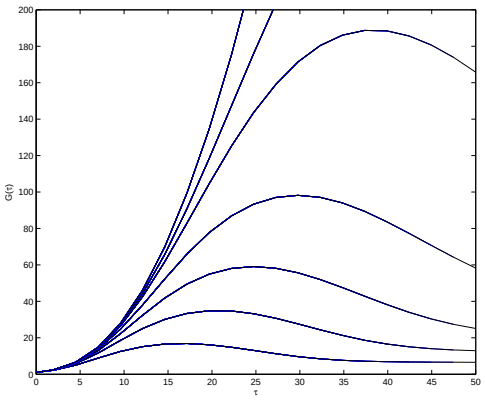

Figure 1: Gain curves for the Batchelor vortex with $(n, q, k) = (-2, 3, 0.3)$. Reynolds numbers Re^* are, from lower to higher curve: $2 \times 10^3, 5 \times 10^3, 10^4, 2 \times 10^4, 5 \times 10^4, 10^5, 10^6$.

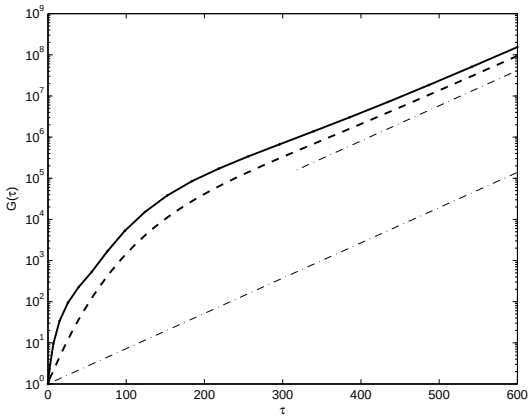

Figure 2: Gain curve for the Batchelor vortex. $(n, q, k) = (-1, 2, 0.268)$, $Re^* = 1.74 \times 10^5$ (solid line). The legend of the other curves is explained in the text.

we report the growth function for the Batchelor vortex for various Reynolds number values and for $(n, q, k) = (-2, 3, 0.3)$. The figure basically reproduces the viscous results presented in Fig. 6 of [3] and the results seem to be accurate within plotting accuracy. The curves displayed in this figure have been computed by the direct-adjoint iteration employing $N = 100$ spatial discretization points. The solid line displayed in Fig. 2 which reproduces Fig. 1 of [4] has also been obtained with this technique and the results seem to be accurate as well.

The code involving diagonalization and matrix exponentiation was first successfully validated on the Hagen-Poiseuille velocity profile, and on data reported in [13]. The situation with the Batchelor vortex is, however, quite different. We were only seldom able to perfectly reproduce transient growth data, published in [3] and [4], obtained with direct-adjoint method by introducing in the optimization procedure only converged eigenmodes. In Fig. 2 we report the growth function calculated with this technique as a dashed line, while the dot-dashed line is the slope of the more unstable viscous mode. The number of eigenfunctions employed in order to calculate this gain curves is the maximum number of converged eigenfunctions we were able to extract with our code. In Fig. 3 and 4 we report the spectrum of the discretized operator for the same data of Fig. 2, for two different numbers of collocation points by employing the two-equations model. Filled dots indicate converged eigenvalues and circles spurious ones. For the case considered our best efforts allow us to extract a number of $N_e = 23$ eigenfunctions. As is clearly seen from Figs. 2, the superposition of these modes is not able to correctly reproduce the initial trend of the gain curve, which depends on the inviscid continuous spectrum [4]. On the other hand, if one introduces in the optimization procedure the right branch of eigenvalues denoted by circles, the calculated growth function accurately fits the ones calculated with the more expensive "direct-adjoint" procedure. All the gain curves shown hereafter have been calculated with the diagonalization procedure, applied to the four-variables model. The results has been compared with those obtained with the "direct-adjoint" procedure on a coarser set of the parameters values.

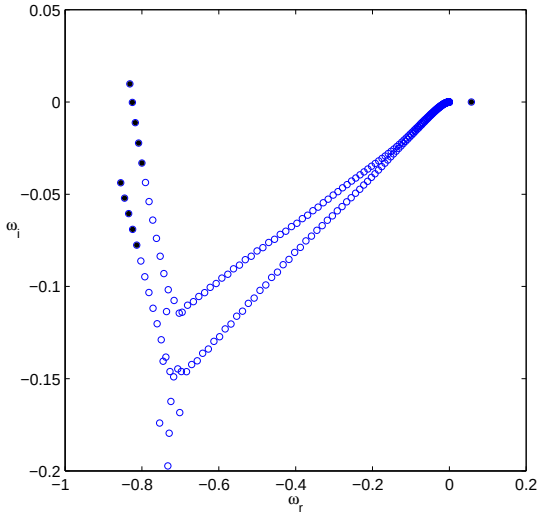

Figure 3: Spectrum of the Batchelor vortex. $(n, q, k) = (-1, 2, 0.268)$, $Re^* = 1.74 \times 10^5$, $N = 180$.

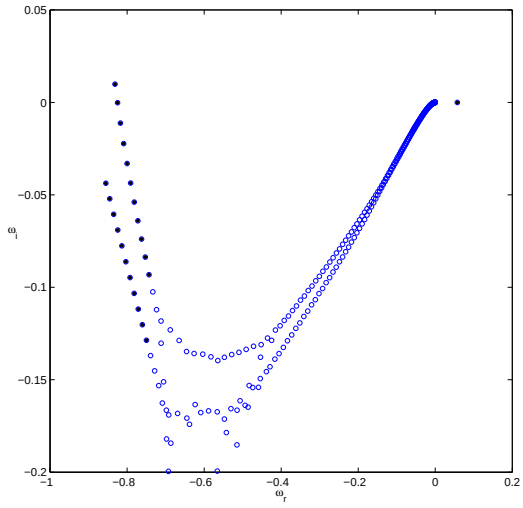

Figure 4: Spectrum of the Batchelor vortex. $(n, q, k) = (-1, 2, 0.268)$, $Re^* = 1.74 \times 10^5$, $N = 250$.

4 RESULTS

Since a major aim of the present paper is to investigate the competition between exponential instabilities and transient growths, we firstly calculated both instabilities in a wide portion of the $q - k$ plane for different Reynolds numbers. The results in Fig. 5 shows the topography of both instabilities, ranging from sufficiently high but finite swirl numbers and axial wavenumbers to the limit of Gaussian jet and very long axial wavelengths, for helical $(n = \pm 1)$ and double-helix $(n = \pm 2)$ modes and $Re = 10^4$. For what it concerns the axisymmetric mode $(n = 0)$, although it presents large transient growths at low axial wavenumbers, it is not phisically meaningful because a very long time is needed to achieve the maximum gain. For this reason the related results are not displayed. The use of Re number, based on the axial velocity scale and the dispersion radius of vorticity, allowed us to work in a higher Reynolds number range, exceeding the numerical limitations of previous works [3].

In Fig. 5 the colored regions represent maps of iso-level growth peak, shown as $\log_{10} G_{\max}$, in a $(q - k)$ plane zone where exponential instabilities are not present. These last occupy a fairly small white region where the iso-level growth rate curves are also depicted. The red line of the maps represents the marginal curve for the exponential instabilities in the inviscid case, so as it is calculated with our code. Although the present region of inviscid instability appears less extended as compared to the one calculated with a different technique by [8], the results are just the same meaningful because the inviscid unstable modes found by [8] beyond our red line are quickly damped at Reynolds number large as much as one likes but finite.

Let us examine the results in Fig. 5 in more details. Firstly we consider the case of double-helix modes $n = \pm 2$. Because of the non-zero axial flow of the Batchelor model the symmetry of flow field is broken and the results for $n = -2$ and $n = +2$ are quite different. For $n = -2$ the figure shows the simultaneous presence of asymptotic and transient growths which occupies

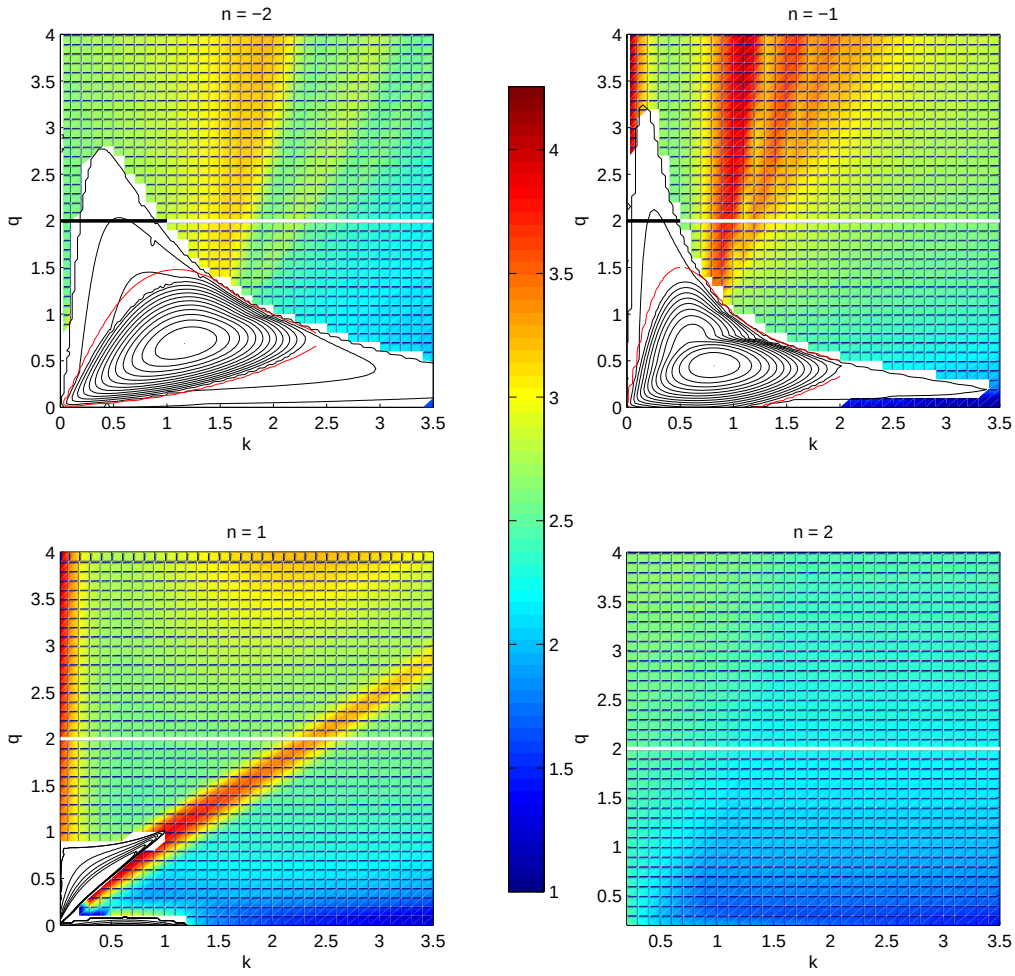

Figure 5: Topography of instabilities and of transient growth results for the Batchelor vortex at $Re = 10^4$ and $|n| = \pm 1, \pm 2$. White regions are of exponential instability. Colored regions are the levels of $\log_{10} G_{\max}$. Explanation of the various curves is given in the text.

different regions of $(q - k)$ plane, the former being of both viscous and inviscid nature. The bulk of the exponential instability region is governed by the coexistence of both kinds of modes, as well as by modes with an hybrid nature; on the other hand, the presence of two purely viscous modes tongues, with weak growth rates and extending both toward large q (and small k) and toward large k (and small q), can be observed. For what it concerns the algebraic growths, one may observe the presence of the central yellow strip where G_{max} attains its maximum values. The mode $n = +2$ shows the complete absence of any exponential instabilities with very low transient growths probably due to the

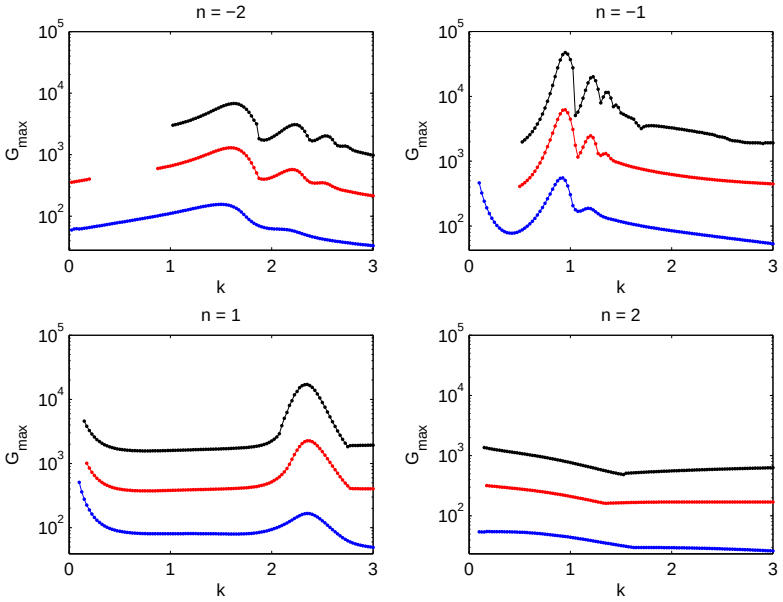

Figure 6: $G_{\max}$ *vs* k for $|n| = \pm 1, \pm 2$ at different Reynolds numbers and $q = 2$. Blue: $Re = 10^3$, red: $Re = 10^4$, black: $Re = 10^5$

action of viscous diffusion which typically dissipates higher-order disturbances. The results relative to the bending modes $|n| = 1$ are quite different. Focusing firstly on the $n = -1$ case, although the exponentially unstable region displays the same two-lobed structure as the case $n = -2$ with the same mixed nature of the modes, the algebraic counterpart presents very large transient growths in the wedge-shaped (red/yellow striped) region and for very long axial wavelengths.

The physical meaning of these two transient effects seems to be different. According to [2] and [3], the high algebraic instabilities in the wedge-shaped region should be due to a 'resonance phenomenon' which occurs when the mean-flow angular velocity advecting the unsteady vorticity matches the frequency of a core mode localized on the symmetry axis. For $Re = 10^4$ the strength and extension of the resonance are more than doubled with respect to results in [3], showing the inviscid character of the transient growths. On the other hand, the large long-wave bending modes growths are attributed to velocity disturbances that do not feel the action of viscosity at high radial distances. However, such modes are not of physical interest because the assumed mean flow is practically no more valid at very large radii due to non-uniformities. The $n = +1$ mode displays the same strong transient growth mechanisms, as shown in Fig. 5, but the resonance, which proceeds roughly along the strip located around $k = 1.1q$, dies away at lower q values, probably because in the adjacent small white region on the left-down corner there is no inviscid but only weak viscous exponential instabilities [6].

Fig. 6 shows the variations of the maximum growths against the axial wavenumber for various Re and $q = 2$, corresponding to the horizontal line in each frame of Fig. 5. The exponentially unstable k-interval is not displayed. As a general trend, G_{max} increases with increasing Re. In

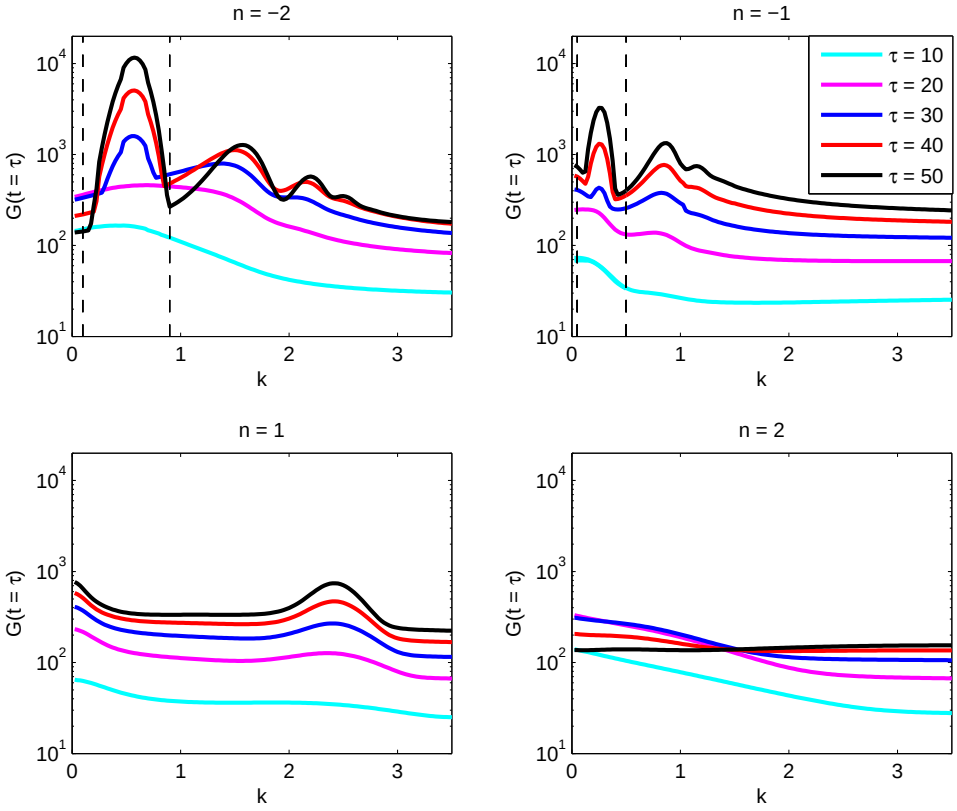

Figure 7: $G(t=\tau)$ *vs* k for $|n| = \pm 1, \pm 2$ for $q = 2$ and $Re = 10^4$.

order to make a comparison between the growth rate of the exponential and non-modal instability mechanisms, Fig. 7 shows the gain peaks at different time instants, for bending and double-helix modes. The two vertical dashed lines spot the exponentially unstable k-range, where it is present. At each instant here considered, the gain is found to be greatest for $n = -2$ mode, caused by asymptotic instabilities which seem are dominant at initial short instants too.

5 CONCLUSIONS

The transient behavior of perturbations in the linear stability analysis of vortex columns with axial flow has been studied by employing both the matrix exponentiation and the direct-adjoint techniques. The competition between weak viscous exponential and transient growths of perturbations has been analyzed in a wide range of the parameters space. The exponential eigenmodes are seen to prevail at all initial short instants considered in our computations.

References

[1] A. Antkowiak and P. Brancher *Transient energy growth for the Lamb-Oseen vortex*. Phys. Fluids Vol. **16** (1), L1–L4 (2004).

[2] D. S. Pradeep and F. Hussain *Transient growth of perturbations in a vortex column*. Journal of Fluid Mechanics, **550**, pp. 251–288 (2006).

[3] C. J. Heaton and N. Peake *Transient growth in vortices with axial flow*. Journal of Fluid Mechanics, **587**, pp. 271–301 (2007).

[4] C. J. Heaton *Optimal growth of the Batchelor vortex viscous modes*. Journal of Fluid Mechanics, **592**, pp. 495–505 (2007).

[5] M. Lessen, P. J. Singh and F. Paillet *The stability of a trailing line vortex. Part 1: Inviscid theory*. Journal of Fluid Mechanics, **63**, part 4, pp. 753–763 (1974).

[6] E. W. Mayer and K. Powell *Viscous and inviscid instabilities of a trailing vortex*. Journal of Fluid Mechanics, **245**, pp. 91–114 (1992).

[7] C. J. Heaton and N. Peake *Algebraic and exponential instability of inviscid swirling flow*. Journal of Fluid Mechanics, **565**, pp. 279–318 (2006).

[8] C. J. Heaton *Centre modes in inviscid swirling flows and their application to the stability of the Batchelor vortex*. Journal of Fluid Mechanics, **576**, pp. 325–348 (2007).

[9] M. Lessen and F. Paillet *The stability of a trailing line vortex. Part 2: Viscous theory*. Journal of Fluid Mechanics, **65**, part 4, pp. 769–779 (1974).

[10] M. R. Khorrami *On the viscous modes of instability of a trailing line vortex*. Journal of Fluid Mechanics, **225**, pp. 197–212 (1991).

[11] D. Fabre and L. Jacquin *Viscous instabilities in trailing vortices at large swirl numbers*. Journal of Fluid Mechanics, **500**, pp. 239–262 (2004).

[12] C. J. Heaton, J. W. Nichols and P. J. Schmid *Global linear stabilty of the non-parallel Batchelor vortex*. Journal of Fluid Mechanics, **629**, pp. 139–160 (2009).

[13] P. J. Schmid and D. S. Henningson *Optimal energy density growth in Hagen-Poiseuille flow*. Journal of Fluid Mechanics, **277**, pp. 197–225 (1994).

[14] R. L. Ash and M. R. Khorrami *Vortex stability* In Fluid Vortices (ed. SI Green), chap. 8, pp. 317-372. Kluwer (1995).

[15] P. J. Schmid and D. S. Henningson *Stability and Transition in Shear Flows*Springer, (2000).

[16] J. A. C. Weideman and S. C. Reddy *A* MATLAB *Differentiation Matrix Suite*. ACM Transactions on Mathematical Software, **26**, 4, p. 465, (2000).